Applied Thermal Engineering 236 (2024) 121848

Contents lists available at ScienceDirect

Applied Thermal Engineering

journal homepage: www.elsevier.com/locate/apthermeng

Research Paper

Experimental analysis of vacuum membrane dehumidifier: Hollow fiber module designs and dehumidification performance

Hye-Jin Cho [a], Seong-Yong Cheon [b], Jae-Weon Jeong [b,*], Gyuyoung Yoon [c,*]

[a] Sustainable Urban Systems Center, Hanyang Institute for Energy and The Environment, Seoul, Republic of Korea
[b] Department of Architectural Engineering, College of Engineering, Hanyang University, Seoul, Republic of Korea
[c] Graduate School of Design and Architecture, Nagoya City University, Nagoya, Japan

ARTICLE INFO

Keywords:
Vacuum-based membrane dehumidifier
Module design
Air-flow channel
Experimental analysis
Dehumidification performance

ABSTRACT

The aim of this study was to experimentally investigate the dehumidification performance of the vacuum membrane dehumidifier with the variance of the air-flow channel in hollow fiber modules. A prototype of a vacuum membrane dehumidifier consisting of five membrane modules was fabricated. The air-flow channel of membrane modules was adjusted by changing an aperture ratio of the module housing that facing the outer surface of hollow fibers. As indicators of dehumidification performance, humidity difference, moisture removal rate, and a pressure loss were considered. A total of 12 experiment sets were designed based on four cases of module configurations and three level of air flow rate to investigate dehumidification performance according to the module configurations. The pressure loss in accordance with the air flow rate for each case were also analyzed based on the additional test results. Finally, a multi-objective optimization analysis was conducted to derive optimal aperture ratios to achieve maximum dehumidification performance and minimum pressure loss. The results showed that the membrane dehumidifier presented 1.06–3.02 g/kg of humidity difference and 28.1–81.8 g/h of moisture removal rate according to the variance of aperture ratio and air flow rate. This indicates that the membrane dehumidifier with lower aperture ratio showed higher dehumidification performance but caused higher pressure loss owing to the longer contacting path between process air and membrane. Moreover, the optimum aperture ratio of membrane module was determined to be 0.2–0.271 m^2/m^2 when providing a higher weight to maximizing the dehumidification performance, while 0.502–0.586 m^2/m^2 aperture ratio is required when predominantly focusing on minimizing pressure loss.

1. Introduction

Recently, the importance of the humidity control in heating, ventilation, and air-conditioning (HVAC) applications has been increase due to the significant decrease in the sensible load in energy-efficient buildings [1–3]. A vacuum membrane dehumidification (VMD) based air-conditioning system has recently emerged as a next generation HVAC system alternative to the conventional vapor compression-based cooling and dehumidification system [4]. A membrane is a perm-selective layer that can penetrate a certain substance in the mixture when there exist the pressure or concentration gradients across the membrane. In a membrane-based dehumidification system, process air is dehumidified by a membrane with high permeability and selectivity to water vapor. The water vapor in process air flowing through the atmospheric side (i.e., feed side) of membrane is absorbed and transferred to the opposite side of membrane (i.e., permeate side) when a total pressure at the permeate side is lowered by a vacuum pump. Because membrane dehumidification process is based on isothermal separation of water vapor from air, a vacuum membrane dehumidification-based air conditioning system can completely separate sensible and latent cooling functions. Decoupled sensible and latent cooling systems can avoid over-cooling and reheating, which may enhance an energy efficiency in thermodynamic aspects compared with the conventional air-conditioning system [5,6].

For decades, existing studies on VMD systems can be classified into three parts: preparation of membrane material for air dehumidification [7–12], investigation on operational characteristics of VMD unit [13–23], and evaluations of energy saving potentials of VMD-assisted HVAC systems [24–27]. In particular, many researchers have focused on exploring operational characteristics of membrane modules under the various feed and permeate side air conditions (e.g., feed air

* Corresponding authors.
E-mail addresses: jjwarc@hanyang.ac.kr (J.-W. Jeong), yoon@yoonlab.net (G. Yoon).

https://doi.org/10.1016/j.applthermaleng.2023.121848
Received 7 July 2023; Received in revised form 19 September 2023; Accepted 23 October 2023
Available online 26 October 2023
1359-4311/

Nomenclature

a_1	Coefficient of viscous force [kg/m^{3}s]
a_2	Coefficient of inertial force [kg/m^{3}s]
A_{mem}	Superficial area of hollow fiber membrane [m^2]
$A_{p,open}$	Open surface area of the membrane modules [m^2]
$A_{p,total}$	Total surface area of the membrane modules [m^2]
b_x	Fixed error
B_y	Propagation of error
D	Diameter [m]
k_m	Mass transfer coefficient of hollow fiber membrane [m/s]
k_{fh}	Permeability of porous media [m^2]
L	Length [m]
M	Mean value
$\dot{m}_{pa}$	Mass flow rate of process air [kg/s]
$\dot{m}_w$	Moisture removal rate [g/h]
N_{slit}	Number of air-passing slits on membrane module [-]
NTU_m	Number of mass transfer units [-]
P	Pressure [kPa]
P_y	Random error
$\dot{Q}_{pa}$	Volumetric flow rate of process air [m^3/h]
S_r	Standard deviation
T	Temperature [°C]
U_y	Overall uncertainty
v	Air velocity [m/s]
w	Weight factor
x_{ap}	Aperture ratio of membrane module [m^2/m^2]

Greek Symbols

β	Forchheimer coefficient [m^{-1}]
ρ	Density [kg/m^3]
ω	Humidity ratio [g/kg$_a$]

Subscripts

in	Inlet
module	Membrane module
pa	Process air
out	Outlet
slit	Air-passing slit on membrane module

Abbreviations

CFD	Computational fluid dynamic
HMA	Hybrid metaheuristic algorithm
HVAC	Heating, ventilation, and air-conditioning
MOGA	Multi-objective genetic algorithm
RMSE	Root mean square error
VMD	Vacuum membrane dehumidification

temperature, humidity ratio, air flow rate, and permeate side pressure) via theoretical approaches. Bui et al. [15,16] performed a thermodynamic analysis of the VMD system by using equations that can interpret gas solution diffusions with a finite difference numerical methods, and they investigated the lower and upper limits of the coefficient of performance (COP) under isentropic and isothermal pump operating conditions. Their results demonstrated that the VMD system in isothermal process could showed 2.5 times higher COP than that of the isentropic process. Cheon et al. [17] suggested a simplified effectiveness and number of transfer unit model for the VMD unit by utilizing the results of numerical simulation and test data. Their results also demonstrated that the membrane selectivity and the number of mass transfer unit exhibited strong impacts on the dehumidification performance of VMD unit.

Some of researchers have fabricated prototypes of VMD systems and examined their operating performance via a series of experiments [19–21]. Bui et al. [19] built a lab-scale vacuum membrane dehumidifier which was composed of a flat-sheet membrane module, and they examined its energy performance via theoretical and experimental approaches. They demonstrated that the COP of the proposed membrane dehumidifier under the isentropic conditions ranged between 2 and 3 under the isentropic conditions. Bui et al. [20] also fabricated a prototype vacuum membrane dehumidifier which consisting of a PVA/LiCl-layered polyetherimide hollow membrane module with an effective area of 3 m^2, and its operating performance was experimentally investigated. Their results showed that the prototype unit showed attainable percentage of moisture removal was up to 86 %, and they also indicated that hollow fiber structured membrane module provided similar dehumidification performance to the flat-sheet membrane with more compact size owing to its higher specific surface area per module volume [28]. Cheon et al. [21] developed a prototype of a hollow fiber membrane-based vacuum membrane dehumidifier with 100 m^3/h of the design air flow rate, and its dehumidification performance in accordance with operating parameters and its transient operating behaviors were experimentally explored. Their results presented that the air flow rate and humidity ratio are the most influential factor on dehumidification performance and COP, and they also showed that the VMD unit can rapidly provide isothermal dehumidification owing to its ability to generate a rapid pressure differential between the feed side and the permeate side.

Meanwhile, there are few studies that investigated the effects of geometrical factors (e.g. air-flow channel, membrane arrangement) of membrane modules on an operational performance of VMD units [22,23]. Chun et al. [22] suggested VMD module with wavy membrane sheets, and explored dehumidification performance of VMD module modules with four different wavy membranes via computational fluid dynamic analysis. Their results demonstrated that when the waviness is over 0.06, the VMD module with wavy membrane could enhance the dehumidification performance owing to the increase in the membrane specific surface. Besides, a steeper wavy membrane is beneficial to dehumidification because steeper wavy membrane could generate a higher vertical velocity in wave trough. Li et al. [23] fabricated flat-sheet structured membrane modules with four different serpentine air flow designs (i.e., triple, quadruple, quintuple, and sextuple serpentine flow channel), and experimentally compared their dehumidification performance and pressure loss under the different air flow rates. Their results showed that the membrane module with a quadruple serpentine flow channel was selected as the best serpentine flow design owing to the tradeoff relationship between the dehumidification rate, pressure loss, and vacuum pumping power.

The literature review on VMD systems showed that the air-flow channel is one of the critical geometrical factors on the performance of vacuum membrane dehumidifiers. The suitable design of air-flowing channel in a hollow fiber module can efficiently distribute the water vapor of feed air on the membrane surface, thereby can maximize the dehumidification performance of VMD. However, only few studies focused on the air-channel design of hollow fiber membrane module for the application of VMD system. Consequently, the object of this study is to experimentally explore the effect of flow channel of hollow fiber on the operational characteristics of the VMD modules. In this study, four types of flow channel were considered, and the air-flow channel for each type was adjusted by removing the air-flowing slits on the module housing. A series of experiments were conducted at the certain temperature and humidity ratio of the process air and different inlet air flow rate. As performance indices, the humidity ratio difference between inlet and outlet process air, moisture removal rate, and pressure loss were considered.

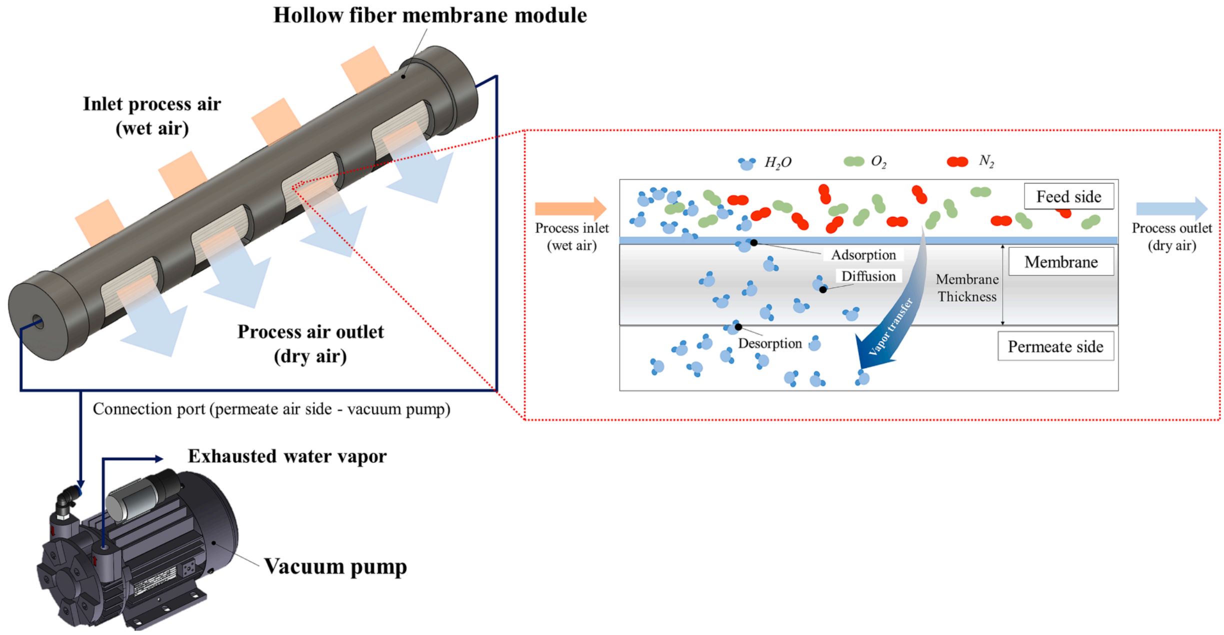

Fig. 1. Schematic of vacuum-based membrane dehumidifier.

2. System overview

2.1. Working principle of vacuum-based membrane dehumidifier

As shown in Fig. 1, a vacuum-based membrane dehumidifier consists of hollow fiber membrane modules and a vacuum pump. A hollow fiber membrane, which is made with a hydrophilic dense membrane, is highly permeable and selective to the water vapor so that can selectively permeate the water vapor of the air flowing through the outer surface of hollow fiber (i.e., feed side), and desorb it across the inner surface of hollow fiber (i.e. permeate side) when there exists the vapor partial pressure differential between feed and permeate sides of membrane. Therefore, when the process air flows through the outer surface of membrane (i.e., feed side) at ambient pressure, and the pressure of the permeate side of air is lowered to a nearly vacuum state by a vacuum pump, the humid process air is dehumidified by a membrane module, and the water vapor which is absorbed from the feed air and desorbed to the permeate side is exhausted to the downstream of a vacuum pump.

From the operating principle of vacuum-based membrane dehumidifier, one can observe that the dehumidification performance of membrane-based dehumidifier is primarily characterized by two factors: the contact area between feed air and membrane where moisture transfer occurs, and the pressure of permeate side which determines the driving force of water vapor transfer from feed to permeate sides. In particular, the contacting area between feed air and membrane determines how many hollow fibers can be installed within a given module volume, and how well the process air contacts with the outer surface of hollow fibers. The air-flowing channel can efficiently distribute the water vapor of feed air on the outer surface of fibers, thus it can maximize the dehumidification performance of membrane module. Therefore, in this study, we have experimentally explored the effects of air flow channel on the operating performance in two aspects: dehumidification performance and pressure loss.

2.2. Design and fabrication of vacuum membrane dehumidifier

In this study, the prototype of vacuum-based membrane dehumidifier was fabricated to investigate the effect of air-flow channel on operating performance. The target air flow rate of feed air was set to 10–30 m^3/h, and the process air temperature and humidity ratio was set to 32 °C and 20 g/kg, respectively, considering the design outdoor air conditions addressed from the local testing standard.

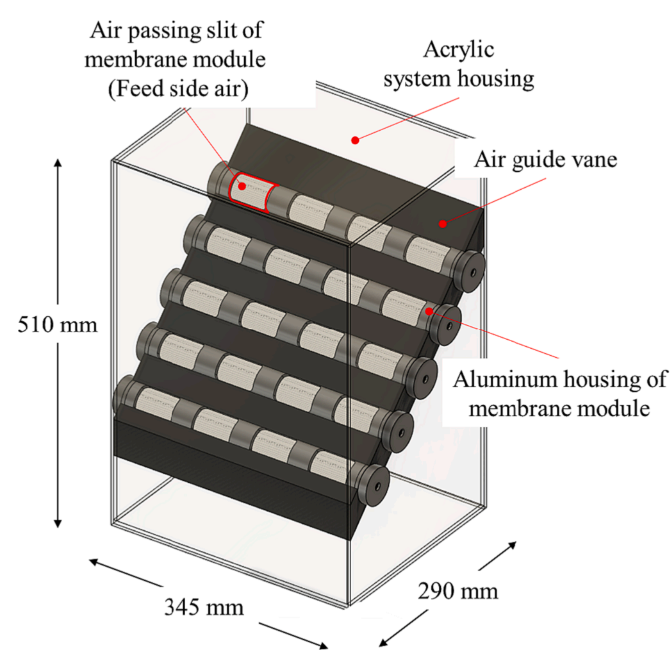

Fig. 2. Three-dimensional diagram of vacuum membrane dehumidifier.

Fig. 2 illustrates of a three-dimensional diagram of prototype vacuum-based membrane dehumidifier. In this study, the commercial hollow fiber membrane module, which is made with polysulfone-based dense membranes with 3,800 hollow fibers was used. The effective length of fiber, which excluding the length of an adhesive to fix the fiber bundles to the module, is 300 mm and fiber outer diameter is 400μ m, respectively. Therefore, the total superficial area of fiber outer side is estimated as 1.3 m^2. The water permeance of the fiber is 620 GPU, which also can be estimated as 5.35×10^{-4} m/s of the overall moisture transfer coefficient (k_m) [21]. In addition, for supplying the process air to the outer surface (or the shell side) of hollow fibers, the housing of membrane module was constructed with a slit opening. The numbers of

Table 1
Physical information of a vacuum membrane dehumidification system.

Component		Properties	Description
Membrane dehumidifier	Module characteristics	Size of membrane dehumidifier	290 mm (Width) × 345 mm (Length) × 510 mm (Height)
		Size of membrane module	30 mm (Diameter) × 345 mm (Length)
		Size of each air-passing slit	30 mm (Width) × 53 mm (Length)
		Number of membrane module	5
		Total surface area of hollow fiber membrane	6.5 m^2 (1.3 m^2 × 5 EA)
	Membrane properties	Membrane material	Polysulfone
		Permeance	620 GPU (1 GPU = 3.35 × 10^{-10} mol/m^2sPa)
		Selectivity	50
		Average pore size	2.5 nm
		Pore thickness	50μ m
		Fiber outer diameter	400μ m
		Effective fiber length	300 mm
Vacuum pump		Pump type	Two-stage rotary vane oil-pump
		Rated Power	0.8 HP (1 HP = 0.745 kW)

hollow fiber membrane module in this study were determined under the condition that the proposed dehumidifier should exhibit number of mass transfer unit (NTU_m) over 1 with 15 m^3/h of the target air flow rate, and the given process air condition. By using Equation (1), the required total surface area of the hollow fiber membrane was estimated to be 6.5 m^2, thus five membrane modules were installed in the dehumidifier in series arrangement. Based on previous study [21], air guide vanes between the membrane modules were installed to insert airflow obstructions to allow process air only to pass through the fibers. To generate the pressure gradient between feed and permeate sides of membrane modules, a rotary vane vacuum pump with oil, which can generate up to 3 kPa of vacuum with the maximum vacuum pump capacity of 0.8 horse power (HP), was employed. Prior to conducting experiments, we have used insert fittings and sealed all joints with silicone to prevent air leakage at the joint parts of the membrane. We have then checked the tightness of the membrane dehumidifier by dropping alcohol on the suspected leak area, and the leaked part was additionally sealed with silicone. Detailed physical information of membrane modules and vacuum pump is listed in Table 1.

$$NTU_m = \frac{\rho_a k_m A_{mem}}{\dot{m}_a} \tag{1}$$

3. Experimental overview

3.1. Experiment apparatus and test conditions

Fig. 3 illustrates an experimental setup of a vacuum-based membrane dehumidifier. The test condition of process air maintained by using an electric heater and a mist humidifier. For considering various amount of air flow rate, a frequency-speed variable fan was installed downstream of process air. In the proposed dehumidifier, when the vacuum pump and the supply air fan are operated, the heated and humidified process air is introduced to the upper side of the membrane dehumidifier (i.e., the process inlet side of the dehumidifier), and the dehumidified air from the lower side of the membrane dehumidifier (i.e., the process outlet side of the dehumidifier) is exhausted.

In this study, four types of air-channel of membrane modules were considered, and the air-flow channel of each membrane module was adjusted by the air-passing slits on the module (Fig. 4). As can be seen in Fig. 4, the flow-direction and the length of air-flow in the membrane module depends on the air-passing slits because process air only can flow into where the slits are open. In this experiment, all slits on the membrane modules were initially covered by the slit-caps, and the slits were sequentially open by removing slit-caps according to the experiment cases; from configuration 1 to 4. Additionally, the slits were removed symmetrically to ensure the uniform distribution of process air. To assess dehumidification performance of the vacuum-based membrane dehumidifier according to the channel of air on the feed side, the aperture ratio of membrane module (x_{ap}) was used as the geometric indicator of the membrane modules. As shown in Equation (2), an aperture ratio is defined as the ratio of the open projection area of membrane modules ($A_{p,open}$) to the total projection area of membrane modules ($A_{p,total}$). $A_{p,total}$ can be obtained with the diameter (D_{module}) and length (L_{module}) of membrane module, and $A_{p,open}$ can be calculated by multiplying the module diameter (D_{module}), slit length (L_{slit}) and the number of opening slit (N_{slit}).

$$x_{ap} = \frac{A_{p,open}}{A_{p,total}} = \frac{N_{slit} \bullet D_{module} \bullet L_{slit}}{D_{module} \bullet L_{module}} \tag{2}$$

Based on Eq. (2), the aperture ratio of each module configuration were as follow: 0.154 m^2/m^2 of aperture ratio (configuration 1), 0.307 m^2/m^2 of aperture ratio (configuration 2), 0.461 m^2/m^2 of aperture ratio (configuration 3), and 0.614 m^2/m^2 of aperture ratio (configuration 4). Observed from Fig. 4, it is expected that the lower aperture ratio would lead to the higher contacting path and contacting time between process air and membrane surface, thus the higher amount of humidity difference between inlet and outlet air. On the other hand, it is expected that the highest amount of pressure loss would cause from the configuration 1, which having the lowest aperture ratio in this experiment, due to the longest air-membrane contacting path among all module configurations.

The measuring point of the prototype unit is demonstrated in Fig. 5. Air temperature and humidity sensors were mounted at the inlet and outlet of the membrane dehumidifier to examine the dehumidification characteristics of the prototype unit. To monitor the flow rate of process air, a vane probe was installed upstream of the prototype unit. Differential pressure sensors were installed at the inlet and outlet process air sides to detect the pressure loss caused by the membrane dehumidifier. The tests were conducted for at least 30 min in each experiment case. Table 2 shows the specifications of the sensors used in this study.

3.2. Experiment indices

As for indices of dehumidification performance, humidity ratio difference (Δω), which is defined as the different between the inlet and outlet humidity ratios (Equation (3), and the moisture removal rate ($\dot{m}_w$), which is a value obtained by multiplying the humidity ratio difference and the mass flow rate of process air (Equation (4), were used.

$$\Delta\omega = \omega_{pa,in} - \omega_{pa,out} \tag{3}$$

$$\dot{m}_w = \dot{m}_{pa}(\omega_{pa,in} - \omega_{pa,out}) \tag{4}$$

The pressure loss caused by the membrane dehumidifier (Δ P) with the variance of the air flow rate was also examined. The pressure loss can be estimated with the measured differential pressure at the inlet and outlet air sides (Equation (5).

$$\Delta P = P_{pa,in} - P_{pa,out} \tag{5}$$

3.3. Uncertainty analysis

Uncertainty analysis was conducted based on the ASHRAE guidance [29] to verify the test results. The overall uncertainty (U_y) of each measured parameter (i.e., temperature, relative humidity, face air

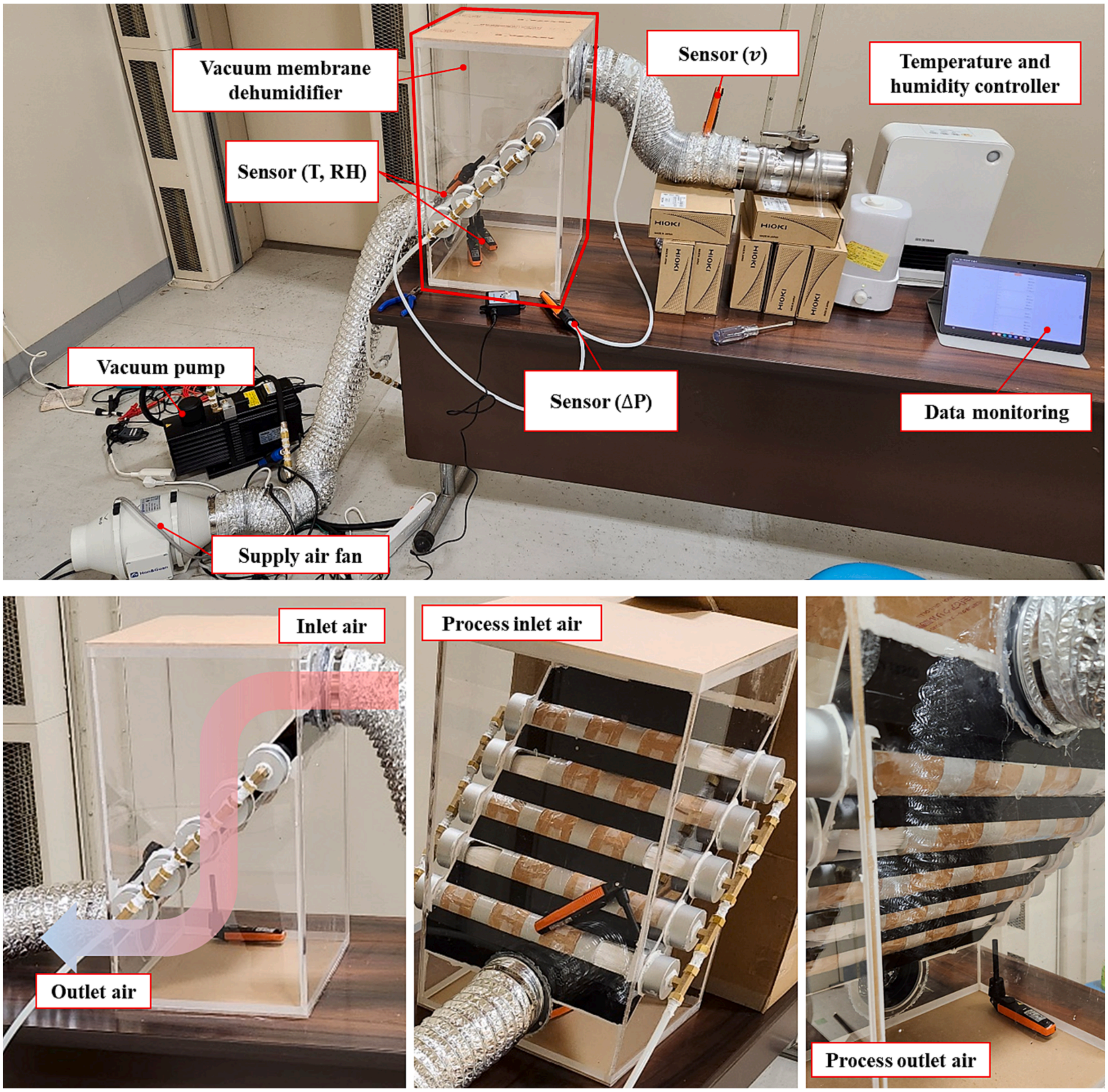

Fig. 3. Overall experimental apparatus of vacuum-based membrane dehumidifier.

velocity, pressure of the inlet and outlet process air) and each performance index (i.e., humidity ratio difference, moisture removal rate, pressure loss) was estimated by the propagation of error (B_y) and the random error (P_y), as indicated in Equation (6). B_y is estimated by using the fixed error (b_{x_i}), which is derived from the standard deviation of the measured data (S_r) and the sensor error (Equation (7). P_y was determined by the S_r and the mean value of the collected data (M) (Equation (8). The overall uncertainty values for each experiment case are summarized in Table 3. As shown in Table 3, the overall uncertainties of all measured and calculated parameters were within in the range of 5%, which is acceptable value in the experiment.

$$U_y = \sqrt{{B_y}^2 + {P_y}^2} \quad (6)$$

$$B_y = \sqrt{\sum_{i=1}^{n}\left(\frac{dy}{dx_i}b_{x_i}\right)^2} \quad (7)$$

$$P_y = \frac{2S_r}{\sqrt{M}} \quad (8)$$

4. Experimental results

4.1. Effect of air flow channel on the dehumidification performance

In this study, all experiments were carried out under the air condition of 32 °C and 20 g/kg of humidity ratio; which is the design outdoor air condition for testing and estimating the cooling capacity of the air-conditioning unit in Korea, and the this standard is addressed by Korean Industrial Standards [30]. In addition, the air flow rate of the vacuum membrane dehumidifier, which is the key factor for determining NTU_m, was considered as the main independent parameter. The test condition of air flow rate ranged from 15 to 30 m^3/h to meet 0.5–1 of NTU_m. Additionally, the air flow rate was set to three level considering the non-linear dehumidification characteristics according to the air flow rate [21]: 15 m^3/h (minimum value), 22.5 m^3/h (intermediate value), and 30 m^3/h (maximum value). Therefore, as listed in Table 4, a

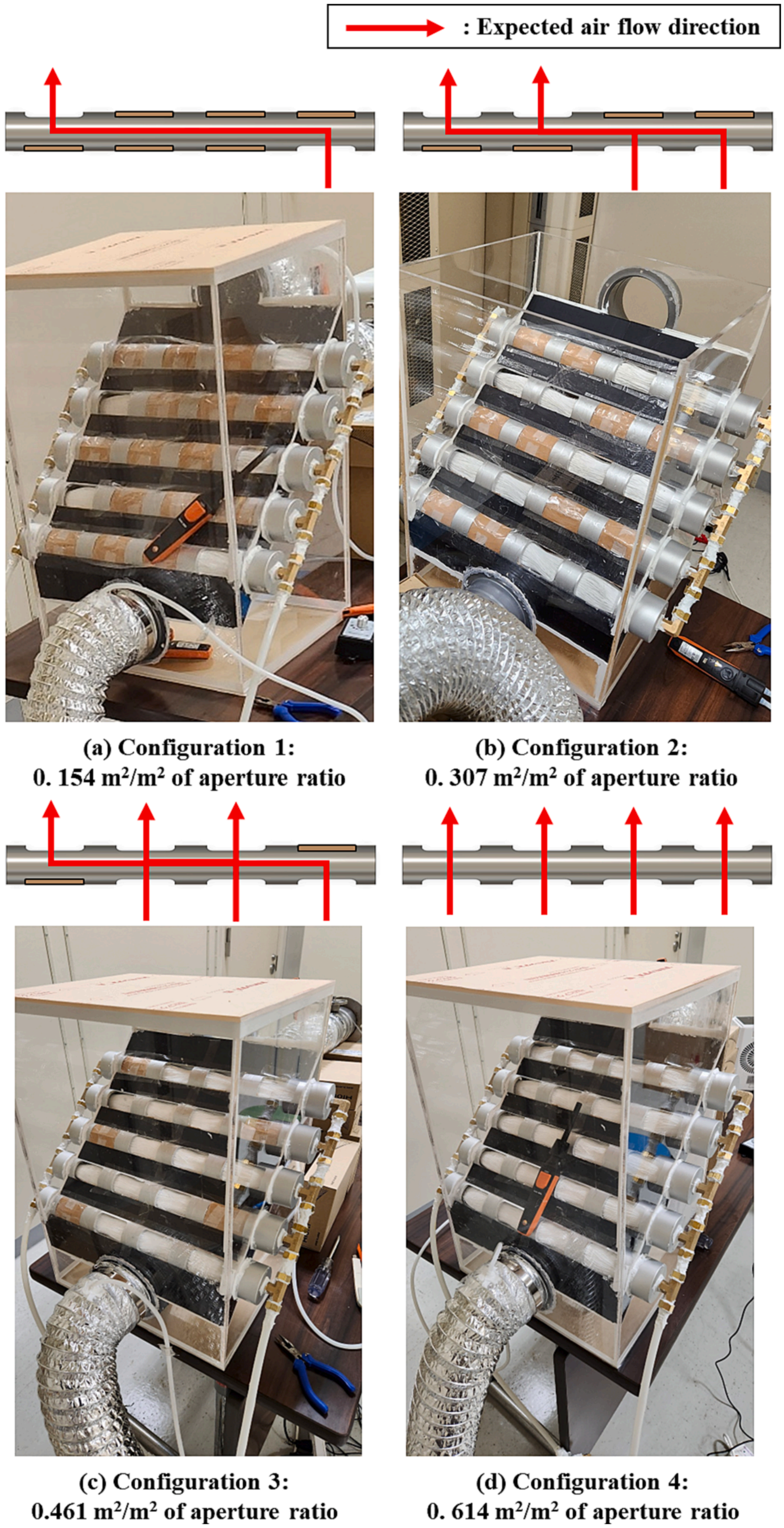

Fig. 4. Comparison of air path configuration according to aperture ratio.

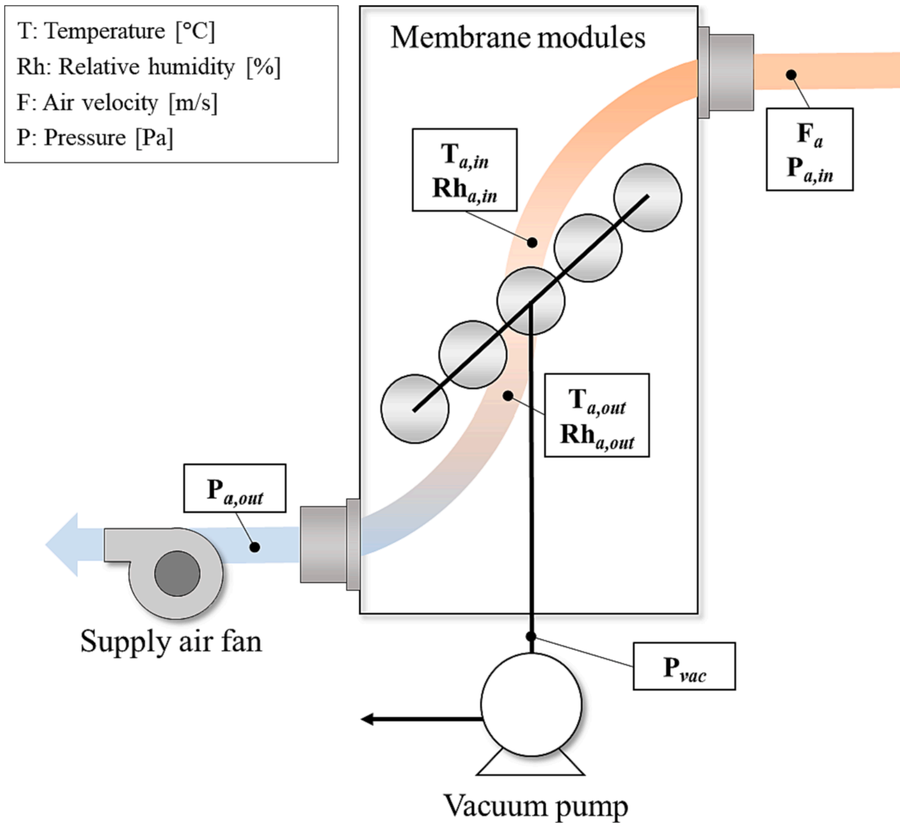

Fig. 5. Measuring points of the prototype.

Table 2
Specifications of the measurement devices.

Variable	Sensor type	Range		Accuracy
Air temperature & relative humidity	Thermo-hygrometer	Temperature	−20 to 60 °C	±0.5 °C
		Humidity	0 to 100%	±1.8%
Air flow rate	Vane probe (Ø100 mm)	0.1 to 15 m/s		±0.1 m/s
Pressure loss	Differential pressure sensor	−150 to 150 hPa		±0.05 hPa

Table 3
Overall uncertainty of measured parameters and performance indices.

Overall uncertainty [%]				
Parameter	Experimental cases			
	Case 1	Case 2	Case 3	Case 4
$T_{pa,in}$	0.367	0.127	0.210	0.096
$T_{pa,out}$	0.094	0.081	0.106	0.034
$\omega_{pa,in}$	5.31	3.264	3.581	4.007
$\omega_{pa,out}$	4.06	3.103	5.506	3.383
$\dot{m}_a$	1.166	1.112	1.187	2.105
$\Delta\omega$	4.687	3.184	4.544	3.695
$\dot{m}_w$	2.187	1.986	2.838	2.895

total of 12 experiment sets were designed considering four types of air-flow channel and three cases of air flow rate. A vacuum pump used in this study was operated at constant rated power, but the permeate side of pressure for each module configuration were different: 10 kPa of average permeate side of pressure for the first module configuration, 8.1 kPa for the second module configuration, 7.7 kPa for the third module configuration, and 7 kPa for the fourth module configuration. Since the vacuum pressure has a low effect on the operating performance of VMD systems when the vacuum pressure is above 4 kPa [15,17], the vacuum pressure was not considered as an independent parameter in this study.

Table 4
Test conditions.

Independent parameter	Level	Range
Aperture ratio of membrane modules	4	0.154, 0.307, 0.461, 0.614 m^2/m^2
Volumetric flow rate of process air	3	15, 22.5, 30 m^3/h
Air condition: 32 °C of temperature, 20 g/kg of humidity ratio		

Fig. 6 demonstrate the effects of the air-path channel on the humidity difference (Fig. 6a) and the moisture removal rate (Fig. 6b). The x-axis of each figure indicates the type of air-path channel of membrane modules, and the y-axis shows the performance indices which were defined in this study. The black, blue, and red symbols in figures indicate the test results for each module configuration when supplying 15, 22.5, and 30 m^3/h of process air to the vacuum membrane dehumidifier, respectively.

The results in Fig. 6a showed that the humidity difference between inlet and outlet process air varied from 3.02 g/kg to 1.06 g/kg. In addition, these results indicate that the vacuum membrane dehumidifier could dehumidify the process air to the lower humidity ratio when the membrane module having the lower aperture ratio of the module slits. The lower aperture ratio of the module slit could increase the possibility that the introduced process air directly contacts the shell side of hollow fibers without bypassing them, thus the higher amount of water vapor transfer between feed and permeate sides of membrane would occur. On the other hand, one can observe that the higher air flow rate decreases the humidity difference when adopting the identical module configuration. This is because the contacting time between process air and membrane surface area shortens when process air flows with a higher

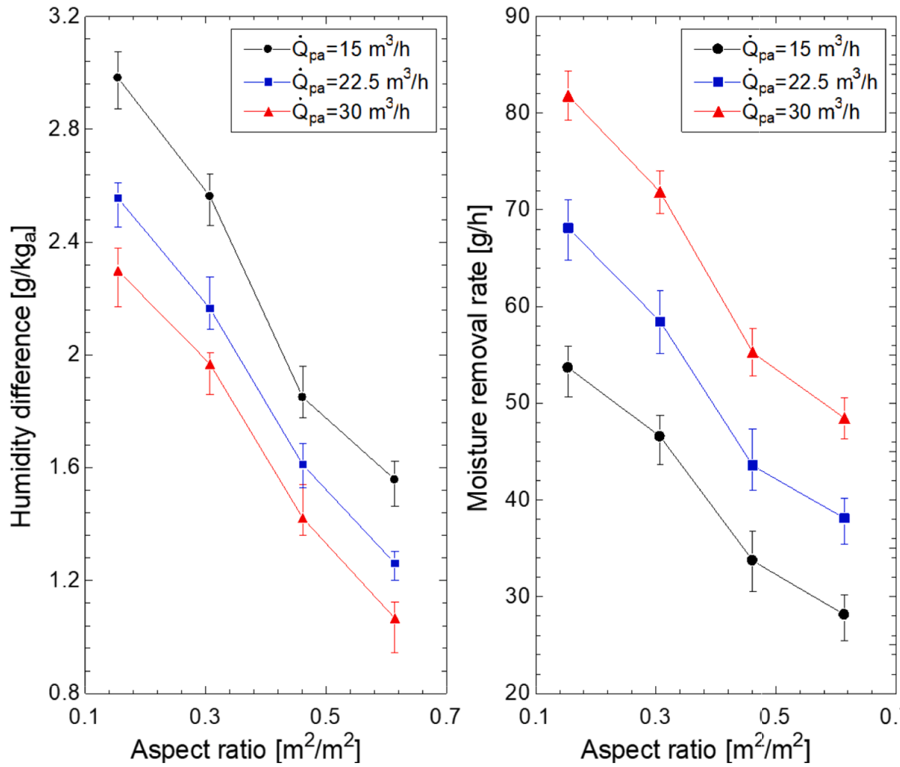

(a) Humidity difference (b) Moisture removal rate

Fig. 6. Comparison of dehumidification performances according to air-flow channel.

face velocity.

As shown in Fig. 6b, the vacuum membrane dehumidifier exhibited 28.1–81.8 g/h of the moisture removal rate during the experiments. Since the moisture removal rate is achieved by multiplying the humidity difference and the air flow rate, the variance characteristics of moisture removal rate according to the module configuration are identical to those of the humidity difference; that is, the vacuum membrane dehumidifier could remove higher amount of moisture when the air-path channel of membrane modules are closed to the first module configuration. On the other hand, opposite to the humidity difference, the higher amount of moisture was removed with the increase in the air flow rate.

From the perspective of the overall operating characteristics according to the module configuration, one can observe in Fig. 6 that all performance indices exhibited nonlinear variations in response to module structure modifications, especially, in the experiment cases 2 to 3. As illustrated in Fig. 4, it was expected that the air-flow direction of the membrane module in case 1 and 2 could be a counter-flow, while that of the membrane module in case 3 and 4 would be a cross-flow. Normally, it is known that effectiveness of a counter-flow heat exchanger is 5–15% higher than a cross-flow configuration [31]. Performance difference according to the flow-configuration was also shown

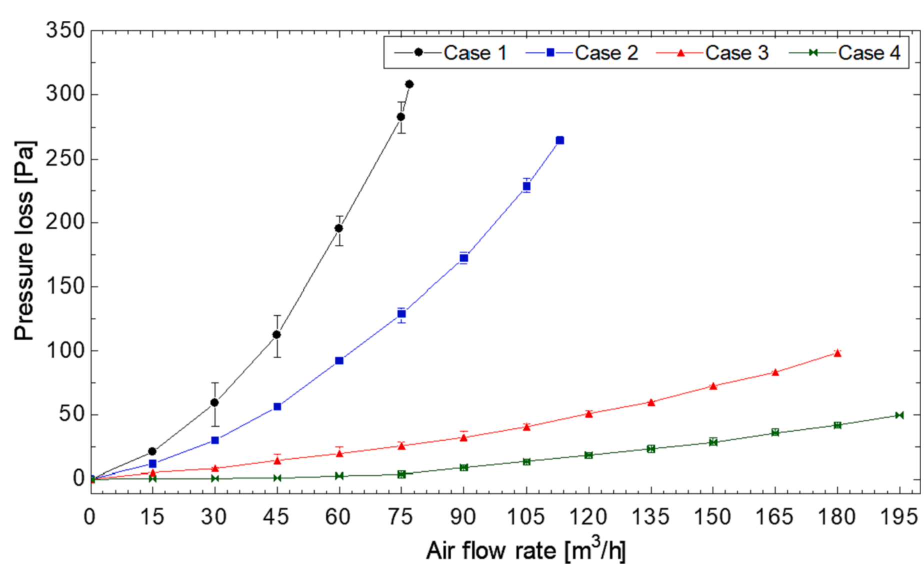

Fig. 7. Comparison of pressure loss in accordance with the face air flow rate.

from the experiment results; the performance indicators were dramatically increased or decreased when the experiment case changed from 2 to 3; while the variance of those from case 1 to case 2, or from case 3 to 4 were much smaller. Therefore, one can conclude that the design of the module housing (e.g., adjustment of aperture ratio of module facing the fiber outer surface) could determine the flow-configuration of the air passing through the fiber outer surfaces, which may enhance or decrease the dehumidification performance under the identical operating conditions.

4.2. Effect of air flow channel on the pressure loss

In this section, the pressure losses generated by each experiment case were compared when the volumetric air flow rate varied from the minimum to maximum operation range of the supply air fan (Fig. 7). Overall, the pressure loss characteristics in the membrane dehumidifier were divided into two groups — "low-air-flow-rate-high-pressure-loss" (membrane modules in case 1 and 2), and "high-air-flow-low-pressure-loss" (membrane modules in case 3 and 4). The membrane dehumidifier in case 4 exhibited the most extensive fan operating range among four cases, with a maximum air flow rate of 195 m^3/h. It also demonstrated a pressure loss of 50 Pa when it operated at the maximum air flow rate. Similarly, the fan in case 3 could supply process air to the membrane dehumidifier up to 180 m^3/h, and the maximum pressure loss in case 3 was 98 Pa. On the other hand, the operating ranges of supply air fan in case 1 and 2 drastically decreased, with a maximum air flow rate of 77 and 119 m^3/h, respectively. Contrary to the air flow rate, the pressure losses in case 1 and 2 significantly increased, with a maximum pressure loss of 308 and 265 Pa, respectively.

In case 3 and 4, the hollow fibers surrounded by the module housing were highly exposed to the atmosphere. This led to an increase of net-cross sectional area of the air flow, thus the resistance of the air flowing to the membrane module decreased Additionally, it was discovered that the higher opening ratio of the module housing (cases 3 and 4) allowed the process air to be introduced from the open air flowing slits directly to the opposite side, which leads to a shorter flow path and less pressure loss. On the other hand, in cases 1 and 2, the introduced air initially flowed in the horizontal direction of the fibers until the process air arrived at other air-flowing slits on the opposite side, and then the air was exhausted to the outside. Hence, the flow path of process air was longer than that of cases 3 and 4, which led to the increase in the resistance of the air to flow and the pressure loss.

4.3. Relationship between aperture ratio and coefficients of viscosity and inertia

Meanwhile, a curve-fitting of pressure loss can be used to comprehend the characteristics of water vapor molecules and fluid flow in the membrane module in a computational fluid dynamic (CFD) analysis [32,33]. In CFD analysis, a hollow fiber membrane module can be assumed as a porous medium [34], and the mass transfer and fluid behaviors in the membrane module are simulated based on the continuity and Navier-Stokes equations. The permeability (k_{fh}) and Forchheimer coefficient (β) of medium are commonly used in two governing equations of a fluid flow within a porous medium [35]. k_{fh} represents the ease with which a fluid flows through the medium, thus the lower k_{fh} causes the higher viscous resistance of the fluid to pass through the porous medium. β means the inertial coefficient in the medium, thereby the higher β leads to the higher inertial drag when fluid flowing through the medium.

Prior to obtain k_{fh} and β of process air for each case, we have derived four quadratic curve fittings of pressure gradient ($-\frac{dP}{dL}$) as a function of face air velocity (v) (Fig. A1 in Appendix) based on Forchheimer's equation (Equation (9) by using the measured pressure loss (Fig. 7) [36]. As can be seen in Fig. A1, the coefficients of viscous force (a_1) and inertial force (a_2) were obtained from the four curve fittings of pressure gradients. Subsequently, k_{fh} and β for each case were estimated with the of viscosity (μ) and density (ρ) of process air. Table 5 listed the values of k_{fh} and β for each case.

Table 5
Comparison of k_{fh} and β according to module configurations.

	Case 1	Case 2	Case 3	Case 4
Permeability of medium (k_{fh})	$2.55 \bullet 10^{-7}$	$2.83 \bullet 10^{-7}$	$9.49 \bullet 10^{-7}$	–
Forchheimer coefficient (β)	107.4	36.59	4.97	3.89

$$-\frac{dP}{dL} = a_1 \bullet v + a_2 \bullet v^2 = \frac{\mu}{k_{fh}} v + \frac{1}{2} \rho \bullet \beta \bullet v^2 \tag{9}$$

As aforementioned, k_{fh}, which is the first order coefficient of pressure loss equation, is an indicator how well the intake air can pass from the membrane module through the area not in contact with the membrane. That is, the lower k_{fh} generates the higher pressure loss, while leads to the lower dehumidification rate, which corresponds to case 1 and 2. k_{fh} even cannot be derived from test data when the intake air is too easy to pass through the membrane module, thus few dehumidification and pressure loss occur. This phenomenon corresponds to result of case 4. As can be seen in Fig. 7, the variance of pressure loss in case 4 was very small than other cases no matter how much the air flow rate increases, but it showed the lowest dehumidification performance. β, which is the second order coefficient of pressure loss equation, is an indicator of energy loss due to that the introduced air to be given kinetic energy to get out of the membrane module. Therefore, the longer air path in a membrane module, which corresponds to case 1 and 2, acts as an obstacle that air passes through the membrane modules.

In short, one can see that the tendency of viscous and inertial resistance according to the aperture ratio of membrane module match well with the experiment results in Section 4.1 and 4.2. In addition, the aperture ratio of membrane module showed tradeoff relationship between dehumidification rate and pressure loss. In the next section, a multi-objective optimization analysis of aperture ratio on the dehumidification and pressure loss was conducted based on the test results.

5. Discussion: Optimal aperture ratio of membrane module

To determine the optimal aperture ratio of the membrane module, a multi-objective optimization analysis was carried out by using the commercial optimization software (PIAnO). PIAnO program has been widely used in that provides design methodology including designs of experiments, meta-modeling and optimization algorithms [37–39]. In terms of design problem formulation, an aperture ratio of membrane module (x_{ap}) and air flow rate ($\dot{Q}_{pa}$) were chosen as design variables. As an objective function for representing the dehumidification performance, the humidity difference (Δω) was adopted, and a pressure loss (ΔP) was considered as a second objective functions for representing the fan working load of a vacuum membrane dehumidifier. The object functions and constraints for the optimization were as follows (Equation (10):

$$\begin{cases} \text{Maximize} \quad : \Delta\omega = f_1\left(x_{ap}, \dot{Q}_{pa}\right) \\ \text{Minimize} \quad : \Delta P = f_2\left(x_{ap}, \dot{Q}_{pa}\right) \\ \qquad\qquad 0.154 \leqslant x_{ap} \leqslant 0.614 \\ \text{Subject to} : 15\ m^3/h \leqslant \dot{Q}_{pa} \leqslant 30\ m^3/h \end{cases} \tag{10}$$

Experiment data of humidity difference and pressure loss in Section 4.1 and 4.2 were utilized for developing meta-models. In the PIAnO program, the meta-model for predicting humidity difference and

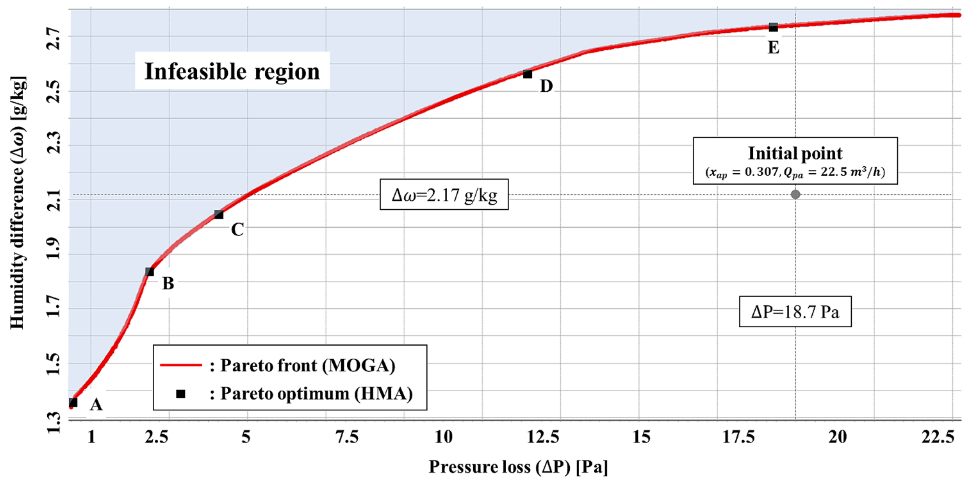

Fig. 8. Pareto front of a multi-objective optimization for a membrane dehumidifier.

Table 6
Design variables and objective functions for each Pareto optimum point.

	Point A ($w_1 = 0.1$, $w_2 = 0.9$)	Point B ($w_1 = 0.3$, $w_2 = 0.7$)	Point C ($w_1 = 0.5$, $w_2 = 0.5$)	Point D ($w_1 = 0.7$, $w_2 = 0.3$)	Point E ($w_1 = 0.9$, $w_2 = 0.1$)
x_{ap} [-]	0.586	0.502	0.459	0.271	0.2
$\dot{Q}_{pa}$ [m^3/h]	21	15.3	15.2	15	15
$\Delta\omega$[g/kg]	1.36	1.83	1.96	2.58	2.75
ΔP[Pa]	0.5	2.45	3.36	12.3	18.1

pressure loss, which exhibited 0.1080 g/kg and 0.6172 Pa of root mean square error (RMSE) values for model validation data, were derived as shown in Fig. A2. Developed *meta*-models was then used to provide optimization solutions suited for the type of design problems by automatically calculating and analyzing the performance indices in PIAnO program. As shown in Figs. 6 and 7, humidity difference and pressure loss showed non-linear behaviors according to variance of aperture ratio. To solve non-linear problems, multi-objective genetic algorithm (MOGA), which is one of the most popular global optimization methods that can generate a well-spread Pareto front for multi-objective functions [40], was adopted. In addition, Pareto optimum point according to the weight value for each objective function were derived by using hybrid metaheuristic algorithm methods (HMA) [41].

The optimization results are plotted on Fig. 8 in two methods; Pareto-front and the local Pareto optimum. In Fig. 8, the red and line black dots indicate the result of Pareto-front and the local Pareto optimum solution, respectively. The blue region in Fig. 8, which is above the red line, indicates that the solutions for humidity difference and pressure loss cannot exist in this region. For example, when a gray point which operated with 0.307 m^2/m^2 of aperture ratio and 22.5 m^3/h of air flow rate is considered as an initial point, a vacuum membrane dehumidifier corresponds with the gray point cannot attain the humidity difference higher than 2.75 g/kg, and the pressure loss lower 5 kPa. In addition, in the local Pareto optimum approach, the aperture ratio and the air flow rate were considered as weight factors (w_1, and w_2, respectively), and design variables and objective functions according to each weight factor were listed in Table 6.

As shown in Fig. 8, all of the optimized points were plotted in the direction of maximizing Δω and minimizing Δ*P*. In addition, Fig. 8 could provide an optimum solution that can have a higher Δω or a lower Δ*P* compared to the initial point which having a 2.17 g/kg of Δω, and 18.7 Pa of Δ*P*. One can observe from Fig. 8 and Table 6 that the optimum with higher aperture ratio and air flow rate points (i.e., Point A and B) was found when considering a higher weight to the Δ*P*. In addition, the results demonstrated that regardless of how little weight is given to the necessity of dehumidification capacity, the aperture ratio of membrane module lower than 0.586 m^2/m^2 should be satisfied. On the other hand, the optimum points with lower aperture ratio and air flow rate (i.e., Point D and E) were revealed when a higher weight to the Δω was considered. Additionally, to avoid an excessive pressure loss from a membrane module, the aperture ratio should maintain at least 0.2 m^2/m^2. Moreover, one can see in Fig. 8 that the Δω changes rapidly between Point A and C, while a large variance in Δ*P* occurred between the Point D and E. When the aperture ratio of membrane module is in the high range (i.e., 0.459–0.586 m^2/m^2), the Δω was strongly impacted by the design variables. On the other hand, the Δ*P* was significantly affected while the Δω was not when the aperture ratio of membrane module is in the low range (i.e., 0.2–0.271 m^2/m^2).

6. Conclusions

This study purposed to experimentally investigate the effect of air-flow channel design in the hollow fiber module on the dehumidification and energy performance of vacuum membrane dehumidifier for HVAC applications. In this study, the air-flow channel of the hollow fiber module was modulated by using air-passing slits, and the aperture ratio of the membrane module was used as an indicator of module configuration. A prototype of vacuum membrane dehumidifier consisting of five hollow fiber modules were constructed, and four types of a vacuum membrane dehumidifier with different air-flow channel were tested.

From the test results of the membrane dehumidifier, this study demonstrated as follows:

- The membrane modules with low aperture ratio (case 1 and 2) presented dehumidification performance (i.e., humidity difference, moisture removal rate) up to 2.9 times higher than those with higher aperture ratio (case 3 and 4). This is because the modules in case 1 and 2, which had an air configuration that was predicted to be near to counter-flow, would have longer contacting path between process air and fibers than the modules in case 3 and 4, which had an air flow configuration predicted to be close to cross-flow.
- On the other hand, the longer contacting path between air and fibers acts as the higher resistance of air to flow in the modules, the membrane modules in case 1 and 2 showed up to 6 times higher pressure loss than those of case 3 and 4 under the identical air flow rate. Additionally, the coefficients of inertial and viscous force for each case, which were derived by the pressure loss data, could represent the tradeoff relationship between dehumidification performance and pressure loss according to the air-flow configuration.

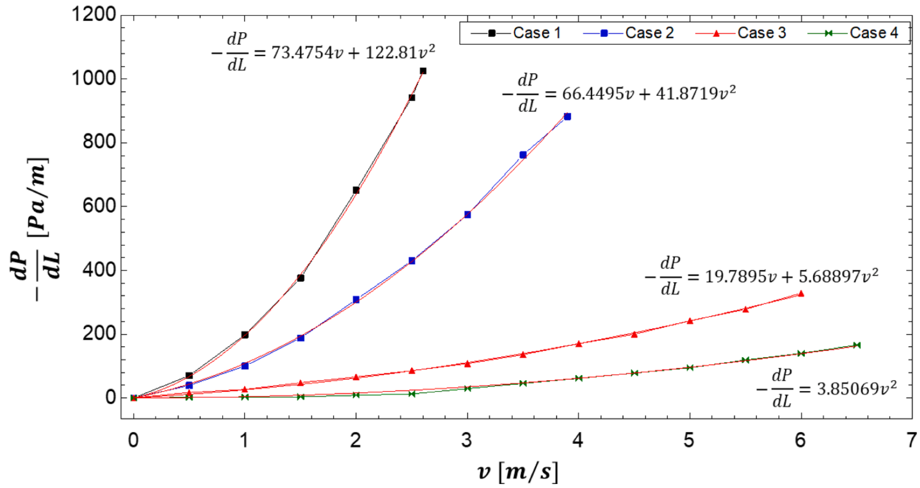

Fig. A1. Curve fittings of pressure loss gradient for four module configurations.

- In multi-objective optimization analysis, it was found that the aperture ratio of membrane module should maintain 0.2–0.271 m^2/m^2 when mainly concentrating on improving dehumidification performance, while the required aperture ratio range is 0.502–0.586 m^2/m^2 when predominantly focusing on reducing pressure loss.

From the results, the air-flow channel on the hollow fiber module plays an important role in determining the dehumidification performance and pressure loss of a vacuum membrane dehumidifier, and the adjustment of an aperture ratio on the module outer surface would be an applicable method to design the hollow fiber modules used for VMD systems. However, there still remains limitation in drawing the design methods when only considering the apparatus ratio as a design parameter because additional design factors of membrane modules (i.e., the array of membrane modules, the shape of air-passing slits) were not considered. Consequently, detailed simulation that can interpret the behaviors of moisture and air in the membrane modules under the various design conditions (e.g., computational fluid dynamic analysis) would be conducted in a future work. Furthermore, this study only focused on the dhimmification characteristics of a vacuum membrane dehumidifier, and a further work should examine the impacts the air-flow channel of the hollow fiber module on the energy efficiency of a vacuum membrane dehumidifier with the advanced vacuum pump control (i.e., invertor control or sequential control of vacuum pumps).

CRediT authorship contribution statement

Hye-Jin Cho: Conceptualization, Methodology, Data curation, Writing – original draft. **Seong-Yong Cheon:** Methodology, Data curation, Validation. **Jae-Weon Jeong:** Supervision, Validation. **Gyuyoung Yoon:** Supervision, Validation.

Declaration of Competing Interest

The authors declare that they have no known competing financial interests or personal relationships that could have appeared to influence the work reported in this paper.

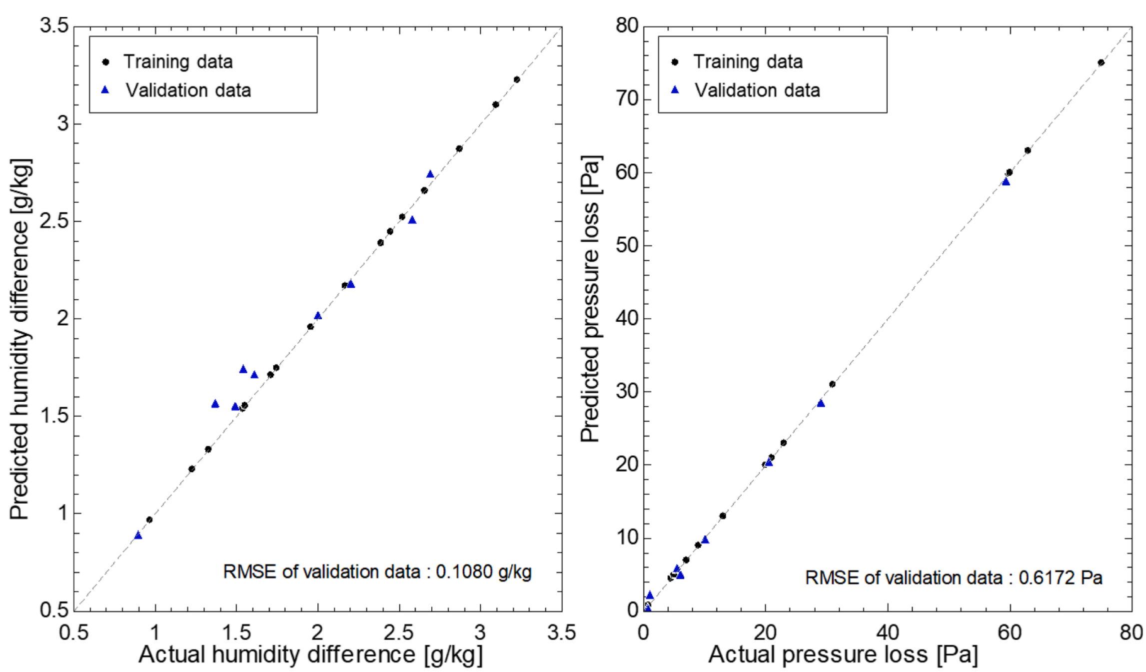

Fig. A2. Comparisons between predicted and actual humidity difference and pressure loss.

Data availability

Data will be made available on request.

Acknowledgements

This work was supported by JSPS KAKENHI [No. 22K04431], JST Sakura Science Exchange Program, and the National Research Foundation of Korea [No. 2022R1A2B5B02001975].

Appendix

See Figs. A1 and A2.

References

[1] J. Woods, N. James, E. Kozubal, E. Bonnema, K. Brief, L. Voeller, J. Rivest, Humidity's impact on greenhouse gas emissions from air conditioning, Joule 6 (2022) 726–741, https://doi.org/10.1016/j.joule.2022.02.013.
[2] J. Winkler, J. Munk, J. Woods, Sensitivity of occupant comfort models to humidity and their effect on cooling energy use, Build. Environ. 162 (2019) 106240.
[3] J. Winkler, J. Munk, J. Woods, Effect of occupant behavior and air-conditioner controls on humidity in typical and high-efficiency homes, Energ. Build. 165 (2018) 364–378, https://doi.org/10.1016/j.enbuild.2018.01.032.
[4] J. Woods, Membrane processes for heating, ventilation, and air conditioning, Renew. Sustain. Energy Rev. 33 (2014) 290–304.
[5] O. Labban, T. Chen, A.F. Ghoniem, J.H. Lienhard, L.K. Norford, Next-generation HVAC: Prospects for and limitations of desiccant and membrane-based dehumidification and cooling, Appl. Energy 200 (2017) 330–346, https://doi.org/10.1016/j.apenergy.2017.05.051.
[6] O.M. Zaki, R.H. Mohammed, O. Abdelaziz, Separate sensible and latent cooling technologies: A comprehensive review, Energy Convers. Manag. 256 (2022), 115380, https://doi.org/10.1016/J.ENCONMAN.2022.115380.
[7] Y. Li, H. Jia, F. Pan, Z. Jiang, Q. Cheng, Enhanced anti-swelling property and dehumidification performance by sodium alginate–poly(vinyl alcohol)/polysulfone composite hollow fiber membranes, J. Memb. Sci. 407–408 (2012) 211–220, https://doi.org/10.1016/J.MEMSCI.2012.03.049.
[8] F.H. Akhtar, M. Kumar, K.V. Peinemann, Pebax®1657/Graphene oxide composite membranes for improved water vapor separation, J. Memb. Sci. 525 (2017) 187–194, https://doi.org/10.1016/J.MEMSCI.2016.10.045.
[9] T.D. Bui, Y. Wong, K. Thu, S.J. Oh, M. Kum Ja, K.C. Ng, I. Raisul, K.J. Chua, Effect of hygroscopic materials on water vapor permeation and dehumidification performance of poly(vinyl alcohol) membranes, J. Appl. Polym. Sci. 134 (2017) 1–9, https://doi.org/10.1002/app.44765.
[10] D.T. Bui, A. Nida, K.C. Ng, K.J. Chua, Water vapor permeation and dehumidification performance of poly(vinyl alcohol)/lithium chloride composite membranes, J. Memb. Sci. 498 (2016) 254–262, https://doi.org/10.1016/j.memsci.2015.10.021.
[11] V. Deimede, D. Vroulias, J. Kallitsis, T. Ioannides, Pyridinium based Poly(Ionic Liquids) membranes with exceptional high water vapor permeability and selectivity, Sep. Purif. Technol. 251 (2020), 117412, https://doi.org/10.1016/J.SEPPUR.2020.117412.
[12] F.H. Akhtar, H. Vovushua, L.F. Villalobos, R. Shevate, M. Kumar, S.P. Nunes, U. Schwingenschlögl, K.V. Peinemann, Highways for water molecules: Interplay between nanostructure and water vapor transport in block copolymer membranes, J. Memb. Sci. 572 (2019) 641–649, https://doi.org/10.1016/J.MEMSCI.2018.11.050.
[13] C. Vallieres, E. Favre, Vacuum versus sweeping gas operation for binary mixtures separation by dense membrane processes, J. Memb. Sci. 244 (2004) 17–23, https://doi.org/10.1016/J.MEMSCI.2004.04.023.
[14] J. Min, M. Su, Performance analysis of a membrane-based enthalpy exchanger: Effects of the membrane properties on the exchanger performance, J. Memb. Sci. 348 (2010) 376–382, https://doi.org/10.1016/j.memsci.2009.11.032.
[15] T.D. Bui, F. Chen, A. Nida, K.J. Chua, K.C. Ng, Experimental and modeling analysis of membrane-based air dehumidification, Sep. Purif. Technol. 144 (2015) 114–122, https://doi.org/10.1016/j.seppur.2015.02.019.
[16] D.T. Bui, M. Kum Ja, J.M. Gordon, K.C. Ng, K.J. Chua, A thermodynamic perspective to study energy performance of vacuum-based membrane dehumidification, Energy 132 (2017) 106–115, https://doi.org/10.1016/j.energy.2017.05.075.
[17] S.Y. Cheon, H.J. Cho, J.W. Jeong, Simplified effectiveness and number of transfer unit model for a vacuum membrane dehumidifier applied to air conditioning, Appl. Therm. Eng. 210 (2022), 118404, https://doi.org/10.1016/j.applthermaleng.2022.118404.
[18] A.J. Fix, J.E. Braun, D.M. Warsinger, A general effectiveness-NTU modeling framework for membrane dehumidification systems, Appl. Therm. Eng. 236 (2024) 121514.
[19] T.D. Bui, Y. Wong, M.R. Islam, K.J. Chua, On the theoretical and experimental energy efficiency analyses of a vacuum-based dehumidification membrane, J. Memb. Sci. 539 (2017) 76–87, https://doi.org/10.1016/j.memsci.2017.05.067.
[20] D.T. Bui, P. Vivekh, M.R. Islam, K.J. Chua, Studying the characteristics and energy performance of a composite hollow membrane for air dehumidification, Appl. Energy 306 (2022), 118161, https://doi.org/10.1016/J.APENERGY.2021.118161.
[21] S.Y. Cheon, H.J. Cho, J.W. Jeong, Experimental study of vacuum-based membrane dehumidifier for HVAC system: Parametric analysis and dehumidification performance, Energy Convers. Manag. 270 (2022), 116252, https://doi.org/10.1016/J.ENCONMAN.2022.116252.
[22] L. Chun, G. Gong, P. Peng, X. Fang, W. Li, X. Shi, X. Chen, Study on the dehumidification performance of vacuum membrane-based dehumidification modules with convex membrane characteristics, Chem. Eng. Res. Des. 182 (2022) 225–236, https://doi.org/10.1016/j.cherd.2022.03.050.
[23] C.H. Li, Z.J. Lin, C.C. Chang, S. Rashidi, W.M. Yan, Experimental study on performance measurement of planar vacuum membrane dehumidifier with serpentine flow channel designs, Alexandria Eng. J. 61 (2022) 10701–10711, https://doi.org/10.1016/J.AEJ.2022.04.017.
[24] H.T. El-Dessouky, H.M. Ettouney, W. Bouhamra, A novel air conditioning system: Membrane air drying and evaporative cooling, Chem. Eng. Res. Des. 78 (2000) 999–1009, https://doi.org/10.1205/026387600528111.
[25] S.Y. Cheon, H.J. Cho, J.W. Jeong, Energy saving potential of a vacuum-based membrane dehumidifier in a dedicated outdoor air system, Energy Convers. Manag. 227 (2021), 113618, https://doi.org/10.1016/j.enconman.2020.113618.
[26] H.-J. Cho, S.-Y. Cheon, J.-W. Jeong, Energy impact of vacuum-based membrane dehumidification in building air-conditioning applications, Appl. Therm. Eng. 182 (2021) 116094.
[27] Y.G.Young, S. Kida, S.Y. Cheon, H.J. Cho, J.W. Jeong, Study on strength measure for latent heat handling ability by using membrane unit, The Society of Heating, Air-Conditioning and Sanitary Engineers of Japan, Chubu, 23 (2022) 2022.
[28] W. Zhao, H. Lu, C. Li, Composite hollow fiber membrane dehumidification: A review on membrane module, moisture permeability and self-cleaning performance, Int. J. Heat Mass Transf. 181 (2021), 121832, https://doi.org/10.1016/J.IJHEATMASSTRANSFER.2021.121832.
[29] ASHRAE Guideline 2-2010. Engineering analysis of experimental data, Atlanta, GA, 2010.
[30] KS 9306, Air-conditioner, Korea Standard Association, 2022.
[31] F.P. Incropera, D.P. Dewitt Introduction to Heat Transfer, third ed., John Wiley & Sons, New York, 1996, p. 416, Chapter 8.
[32] X. Liu, M. Qu, X. Liu, L. Wang, Membrane-based liquid desiccant air dehumidification: A comprehensive review on materials, components, systems and performances, Renew. Sustain. Energy Rev. 110 (2019) 444–466, https://doi.org/10.1016/J.RSER.2019.04.018.
[33] S.C. Park, H.S. Park, H.K. Lee, W.G. Shin, Numerical study on flow characteristics of hollow fiber membrane module for water recovery cooling tower, Trans. Korean Soc. Mech. Eng. B 41 (2017) 537–544, https://doi.org/10.3795/KSME-B.2017.41.8.537.
[34] Z.X. Li, L.Z. Zhang, Flow maldistribution and performance deteriorations in a counter flow hollow fiber membrane module for air humidification/dehumidification, Int. J. Heat Mass Transf. 74 (2014) 421–430, https://doi.org/10.1016/J.IJHEATMASSTRANSFER.2014.03.047.
[35] A.O. Alsaiari, Gas-Gas Separation Using a Hollow Fiber Membrane by Presented to the Graduate and Research Committee of Lehigh University in Candidacy for the Degree of Master of Science in Mechanical Engineering, Lehigh University, 2014.
[36] H. Najmi, E. El-Tabach, K. Chetehouna, N. Gascoin, F. Falempin, Effect of flow configuration on Darcian and Forchheimer permeabilities determination in a porous composite tube, Int. J. Hydrogen Energy 41 (2016) 316–323, https://doi.org/10.1016/J.IJHYDENE.2015.10.054.
[37] C.H. Park, PIAnO (Process Integration, Automation and Optimization) User's Manual 3.6. PIDOTECH, 2013 (2013).
[38] J.J. Lee, J.S. Kim, D.C. Lee, H.K. Chang, C.W. Kim, Design optimization of tab attachment positions and cell aspect ratio to minimize temperature difference in 45-Ah LFP large-format lithium-ion pouch cells, Appl. Therm. Eng. 182 (2021), 116143, https://doi.org/10.1016/J.APPLTHERMALENG.2020.116143.
[39] J. Lee, S. Cheon, J. Jeong, Multi-objective optimization for capacity matching and energy performance of heat-pump-driven liquid-desiccant air-conditioning system, Appl. Therm. Eng. 229 (2023), 120615, https://doi.org/10.1016/j.applthermaleng.2023.120615.
[40] K. Deb, A. Pratap, S. Agarwal, T. Meyarivan, A fast and elitist multiobjective genetic algorithm: NSGA-II, IEEE Trans. Evol. Comput. 6 (2002) 182–197, https://doi.org/10.1109/4235.996017.
[41] H. Yi, Q. Duan, T.W. Liao, Three improved hybrid metaheuristic algorithms for engineering design optimization, Appl. Soft Comput. 13 (2013) 2433–2444, https://doi.org/10.1016/J.ASOC.2012.12.004.